The Effect of Curvature on the Performance and Readability of Passive UHF RFID Tags

Darmindra D. Arumugam [1], Daniel W. Engels [2], and Marlin H. Mickle [3]

[1] Department of Electrical and Computer Engineering
Carnegie Mellon University, Pittsburgh, PA 15213, USA
darumugam@cmu.edu

[2] Department of Electrical Engineering
University of Texas at Arlington, Arlington, TX 76019, USA
dengels@uta.edu

[3] Department of Electrical and Computer Engineering
University of Pittsburgh, Pittsburgh, PA 15261, USA
mickle@pitt.edu

***Abstract*—** In this paper, the effect of curvature on the passive UHF RFID tag is studied. Maxwell's equations are used to depict the typical curved passive tag and are used to study the theoretical limitations of a tag operating under curvatures at its normal axes. This theoretical framework is then used to analyze the typical tag for various curvatures. Here, the analysis is conducted to derive the effect of curvature on the optimal impedances for ASIC load matching, as well as gain. This analytical evaluation is also generalized to describe the shift in center frequency of the tag operation due to tag curvatures. The results derived from this theoretical study on commercially available passive UHF RFID tags are verified with experimental results. It is shown that the curvature of passive UHF RFID tags have a significant impact on the performance and readability at values of $K > \pi/\lambda$, and reaches a breakdown on conformity at curvature values of $K = 4\pi/\lambda$.

***Index Terms*—** Passive UHF RFID, curvature.

I. INTRODUCTION

Recently there has been significant interest in the characterization of passive UHF Radio Frequency Identification (RFID) tags [1-8]. The interest in this area is predominantly spurred by the need to understand the implications that the environment has on the performance of these passive tags. Previous studies have concentrated on internal [9-14], as well as external [15-17] environmental factors, but have often times neglected some of the more obvious details involved in the use of passive tags in the industry. These passive tags operate in the Industrial Science and Medical (ISM) band of 902 MHz to 928 MHz within the U.S., and are governed by the Federal Communications Commission (FCC) for frequency selectivity, power levels, and other requirements. The characteristics of passive tags as studied previously have involved many types of analysis such as the backscatter [9, 10], antenna designs [11-13], as well as the application specific integrated circuits (ASIC) studies. Published works citing curvature in antenna designs have not been put in context of passive RFID tags [18-20], while those that have, concentrate on inductively coupled (HF) antennas [21], or lack clear conclusions regarding the effects of curvature on the performance of passive UHF RFID tags globally [22-25].

This paper is organized as follows: a background on tag curvatures and fundamental electromagnetism is presented in Section II. Section III presents the theory of electromagnetism for the specific case of a curved passive RFID tag in free space. The comprehensive general theory and curvature limitations of passive RFID tags are presented in Section IV along with the theory of general propagation. Here, the results of the theoretical analysis are presented to illuminate the impedance

mismatching, as well as gain variation and operational frequency shifting. An experimental analysis is presented in Section V for RFID tags with various curvature values. In Section VI, the effects of the segmentation process and segment density is discussed on the characterization of passive UHF RFID tags in CEM tools. Finally, a comprehensive conclusion is presented in Section VII.

II. BACKGROUND

The typical passive UHF RFID tag is composed of an antenna and an ASIC, that are connected to each other using a conductive glue or solder, as well as a substrate made of a dielectric material such as PET upon which the antenna and ASIC are affixed (as shown in Fig. 1) and packaged for the complete tag. From an RF stand-point, the radiation elements of this tag antenna are the antenna traces.

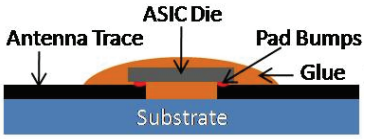

Fig. 1. The typical passive UHF RFID tag with a substrate supporting the antenna and ASIC.

The electrical evaluation for the structure in Figure 1 can be simplified using the assumption that the characteristics of the tag radiation pattern (including frequency selectivity) is dependent predominantly on the tag antenna structure and its matching to the ASIC input terminals [4, 5]. This assumption is further generalized by the fact that the ASIC mis-match is also a static property that would be dynamic in curvature studies, only with respect to the antenna structure. These assumptions allow us to simplify the setup as depicted in Fig. 1, into the traditional antenna studies. Typical commercially available UHF RFID tags tend to have somewhat complex (non-simplistic) current densities. These current variations are an important part of defining the far-field response of the tag itself, as can be viewed from the derived electric far field of Equations 1-3 for the case of a center-fed infinitesimal dipole antenna system with spherical (surface) coordinates.

$$E_r = \eta \frac{I_0 l \cos\theta}{2\pi r^2}\left[1 + \frac{1}{jkr}\right] e^{-jkr} \quad (1)$$

$$E_\theta = j\eta \frac{kI_0 l \sin\theta}{4\pi r}\left[1 + \frac{1}{jkr} - \frac{1}{(kr)^2}\right] e^{-jkr} \quad (2)$$

$$E_\varphi = 0 \quad . \quad (3)$$

Equations 1-3 describe the electric field at every instance in space except at the source itself [26], and are an accurate method for determining the power density and radiation resistance of the tag antenna itself. This system is depicted in Fig. 2, where the tag is considered as a center-fed dipole with a wire length much shorter than the wavelength ($l \ll \lambda$) and is very thin, such that the diameter of the wire is much lesser than the wavelength of the radiated wave ($a \ll \lambda$).

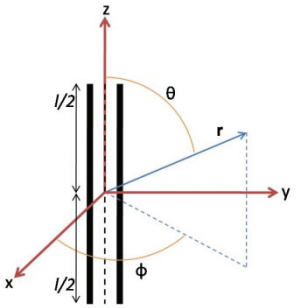

Fig. 2. Geometrical system of the infinitesimal dipole antenna system.

From Fig. 2 and wire antenna theory, we know that the current distribution of the dipole through the entire length of the structure is described using a $\sin\theta$ function, and that depending on the termination at both ends, this function could be altered into a linear (constant slope) function for the short dipole, which allows a simplification that arrives to Equations 1-2. This simplification exists for cases where $l \leq \lambda/50$, which allows us to determine the vector potential with the assumptions that the phase errors are negligible [26, 27] and does not affect the radiation characteristics of the antenna system. Using this justification and assumptions, we can perform the appropriate integration to derive the vector potential using that used by the infinitesimal case in Equation 4.

$$\boldsymbol{A}(x,y,z) = \hat{\boldsymbol{a}}_z \frac{\mu I_0}{4\pi r} e^{-jkr} \int_{-l/2}^{l/2} dz' = \hat{\boldsymbol{a}}_z \frac{\mu I_0 l}{4\pi r} e^{-jkr} \; . \quad (4)$$

The results of this integration are as depicted in Equation 5, where the vector potential is shown to be one half of that shown in Equation 4, and is increasingly accurate as $kr \to \infty$ due to the far field region of the system. Note that the results of this system require that we assume that the current is zero on either ends of the short dipole, and is maximum at the center.

$$\boldsymbol{A}(x,y,z) = \hat{\boldsymbol{a}}_z A_z = \hat{\boldsymbol{a}}_z \frac{1}{2}\left[\frac{\mu I_0 l}{4\pi r} e^{-jkr}\right]. \quad (5)$$

Using Equation 5, we can rewrite Equations 1-3 into Equations 6 and 7, for values of $kr \gg 1$. Here, we see that the approximate simplifications allow us to notice that the fields are half the previous field equations of the infinitesimal dipole as well.

$$E_\theta \approx j\eta \frac{kI_0 l}{8\pi r} e^{-jkr} \sin\theta \quad (6)$$

$$E_r \approx E_\varphi = 0\,. \quad (7)$$

Note that since the directivity is a function of pattern or shape, the directivity and hence the maximum effective capture area of the short dipole is similar to that of the infinitesimal dipole [26, 27]. Following this, the radiation resistance of the short dipole is (squared) one fourth of that of the infinitesimal dipole, and is given in Equation 8. Note that this value is strictly dependent on the length of the dipole as well as the wavelength of the radiated wave.

$$R_r = \frac{2P_{rad}}{|I_0|^2} = 20\pi^2 \left(\frac{l}{\lambda}\right)^2 . \quad (8)$$

III. MATHEMATICAL ANALYSIS OF TAG CURVATURES

From the derivations so far, we notice that the two major changes during curvature are due to the fact that the current distribution would be altered tremendously, and that the geometrical setup would also alter significantly. Curvature can be described effectively using the radius of curvature. This radius of curvature can be depicted using an analogy similar to Fig. 3, where curvature (K) is determined using the radius (R), where $K = 1/R$. From this definition, we can classify curvatures involved in the dipole system to depict the changes as a sum of bent short dipoles.

Fig. 3. Radius of curvature of a wire.

Considering the scenario described by the summation of partially bent short dipoles, it is easily noticed that the current distribution would change drastically as we navigate from one short dipole to the next.

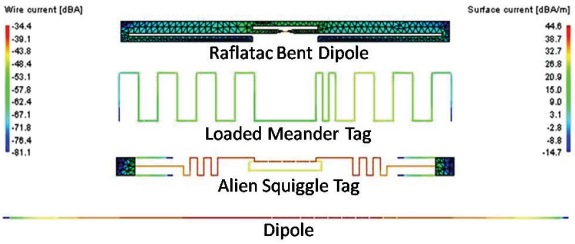

Fig. 4. Current distribution of commercial RFID tags as compared to the typical dipole antenna.

To further explore this condition, Fig.4 depicts the current distribution for three commercially available passive UHF RFID tags as compared to the typical dipole illustrated in Fig. 2, and derived in Equations 1-8.

From Fig. 4, we notice that bends do typically change the current distribution, since they tend to be the radiation echo sites. However, we notice that the linear or log in Fig. 4 (due to dB measure) current distribution patterns for the dipole antenna is best used for the purpose of a generalized theory. In order to model the current distribution, we first depict the scenario under which a curved tag (curved dipole tag antenna) will exist in Fig. 5.

The tag curvature along the radius of curvature (which is equal to the radius of the circle) involves complex manipulations of angles due to the bent short dipoles. In order to properly describe the curvature, we must introduce the angles θ_i', α_i, and β_i as depicted in Fig. 5. These angles are used to depict the study of each dipole with respect to the original short dipole. Note that the use of the summation of short dipoles is similar to that used

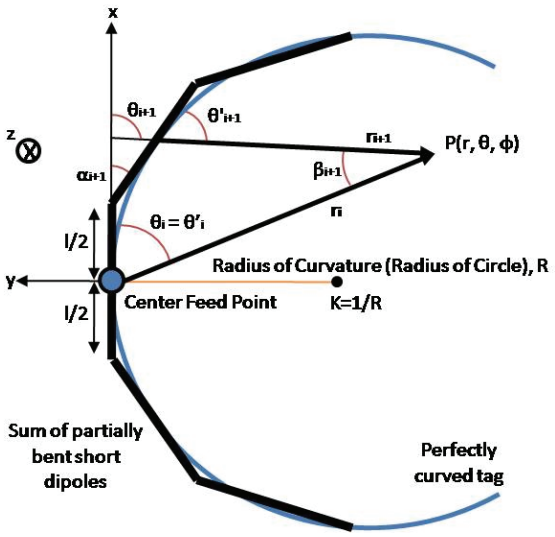

Fig. 5. Geometrical setup of a typical passive UHF RFID tag undergoing z-axial curvature.

in the segmentation process in the methods of moments. From Fig. 5, we can further analyze the triangular nature of the first β angle by utilizing geometrical calculus as depicted in Fig. 6.

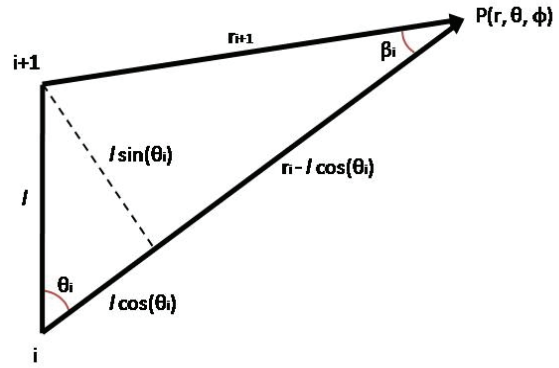

Fig. 6. Geometrical analysis of the far-field pattern angle, $\boldsymbol{\beta}$.

From Figure 6, we notice that the first β angle can be defined by Equation 9, which describes the far-field pattern angle as a subsection of the deployment angle (θ), and the length of each segment during the segmentation process (l). Note that this derivation would be similar to the analysis using computational methods. The results of these computational electromagnetic (CEM) methods will be depicted in subsequent sections.

$$\beta_i = \tan^{-1}\left\{\frac{l\sin\theta_i}{r_i - l\cos\theta_i}\right\} . \qquad (9)$$

Comparing the results obtained in Equation 9 through analysis with Figs. 5 and 6, we notice that the deployment angle of each segment in the curved tag problem can be defined as described in Equation 10, where α is the differential angle between the $(i)th$ segment and the $(i+1)th$ segment as depicted in Fig. 5.

$$\theta_i' = \theta_{i-1}' - \alpha_{i-1} + \beta_{i-1} . \qquad (10)$$

Using the electric far-field derivation in Equations 6 and 7, we can substitute Equation 10 to arrive at the partial solution for the curvature problem. Equations 11 and 12 present the modified field equations that describe the curvature effects on the geometrical nature of the tag antenna.

$$E_\theta \approx j\eta\frac{kI_0 l}{8\pi r_i}e^{-jkr}\sin\theta_i' \qquad (11)$$

$$E_r \approx E_\varphi = 0 . \qquad (12)$$

From Equations 11 and 12, we see that the field equations are complete in terms of the curvature of the system. However, notice that the system still emphasizes a linear current distribution for the entire curved body. This current distribution is non-conformal to the concept of multiple bent short dipoles, and must be modified to depict the current distribution of a set of segments as depicted in Fig. 5. In order to

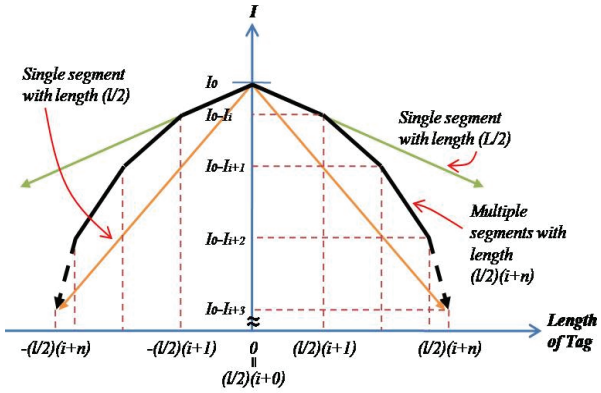

Fig. 7. Current distribution of tag antenna depending on the number of segments and length.

do so, we first review the current distribution of a single dipole element as compared to multiple dipole elements. Fig. 7 shows the current distribution of the single element as compared to the same length dipole with multiple elements.

From Fig. 7, we notice that the current I_0 needs to be modified such that it varies linearly based on the segment number. Here we also see that the current is the same at the either end due to symmetry, and that the current at the end points always approach zero. From this conceptual diagram, Equations 11 and 12 can be effectively modified to resemble Equation 13 and 14, where the current modification as well as the segment length (li) adjustments are considered.

$$E_\theta \approx j\eta \frac{k(I_0 - I_i)li}{8\pi r_i} e^{-jkr} \sin\theta_i' \qquad (13)$$

$$E_r \approx E_\varphi = 0\,. \qquad (14)$$

From Equation 13, we can see that the complexities that exist due to curvature in the far-field can be effectively modeled using geometrical analysis as well as modifications to the current distributions. In the following section, these modifications are used to describe the relevance to propagation, as well as impedance mismatches, gain variations and operational frequency shifting.

IV. CHARACTERISTICS OF CURVED TAGS

In order to study the curvature of the tag, we notice that an explicit simplification is made to the generalized definition of curvature itself. Curvature of the typical tag can be described using $K = 1/R$, where R is the radius of curvature of the entire system. It is easily noticeable, that curvature of the typical passive tag as discussed throughout this paper would be directly related to the differential angle between each segment (α_i) in Fig. 5. To understand the simplification that exist, we must first study the relationship between the effective tag length (L_e) and the radius (R), which can be described using the simple geometry of an arc on a circle as noted in Equation 15.

$$\frac{L_e}{2} = \frac{\theta}{360} 2\pi R\,. \qquad (15)$$

Substituting R for the curvature (K), we can rewrite Equation 15 in the form as depicted by Equation 16.

$$\theta = \frac{360 L_e K}{4\pi}\,. \qquad (16)$$

From Fig. 8, we see that the angle describing the maxima of the arc for the tag effective length is actually described by the deployment angle itself, such that $\theta \equiv \alpha_i$.

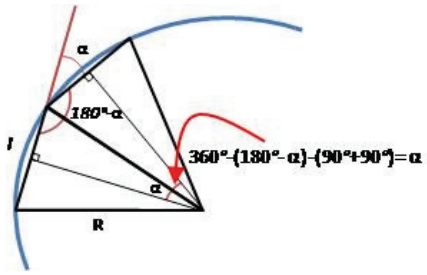

Fig. 8. Relationship between tag effective length ($\boldsymbol{L_e}$) and differential deployment angle ($\boldsymbol{\alpha}$).

Assuming that the deployment angle is constant such that the radius of curvature is constant (the tag is constantly curved, rather than dynamically curved), than we note that $\theta \equiv \alpha$, since $\alpha = \alpha_i = \alpha_{i+1} = \alpha_{i+n}$. This assumption allows us to rewrite θ as a direct substitution of α in Equation 16. Substituting the modified Equation 16 into Equation 10, we get Equation 17.

$$\theta_i' = \theta_{i-1}' - \frac{360 L_e K}{4\pi} + \beta_{i-1}\,. \qquad (17)$$

Finally, substituting Equation 17 into the expanded Equation 13, we derive the complete electric far field relationship for the tag curvature in Equations 18 and 19.

$$E_{\theta_i'} \approx j\eta \frac{k(I_0 - I_i)li}{8\pi r_i} e^{-jkr} \sin\left(\theta_{i-1}' - \frac{360 L_e K}{4\pi} + \beta_{i-1}\right) \qquad (18)$$

$$E_r \approx E_\varphi = 0\,. \qquad (19)$$

In order to understand the implications of the modified field equations, we find the average radiated power in Equation 20 using Equations 18 and 19 [26].

$$W_{rad}(r,\theta_i',\varphi) = \hat{a}_r \frac{1}{2} \times \left[\eta \left| j\frac{k(I_0-I_i)li}{8\pi r_i} e^{-jkr} \sin\left(\theta_{i-1}' - \frac{360 L_e K}{4\pi} + \beta_{i-1}\right)\right|^2\right]. \quad (20)$$

Declaring the radiated power, we use the average radiated power of Equation 20 to define the directivity ($D(\theta_i',\varphi)$) in Equation 21. This is then used to define the radiation and input resistance, as well as the maximum effective area in Equations 21 through to 23 respectively [26].

$$D(\theta_i',\varphi) = \frac{4\pi r_i^2 W_{rad}(r,\theta_i',\varphi)}{\int_0^{2\pi}\int_0^{\pi} W_{rad}(r,\theta_i',\varphi) r_i^2 \sin\theta_i' d\theta_i' d\varphi} \quad (21)$$

$$R_r = \frac{2\int_0^{2\pi}\int_0^{\pi} W_{rad}(r,\theta_i',\varphi) r_i^2 \sin\theta_i' d\theta_i' d\varphi}{|I_0-I_i|^2}, \; R_{in} = \frac{R_r}{\sin^2\left(\frac{kl}{2}\right)} \quad (22)$$

$$A_{em} = \frac{\lambda^2}{4\pi} D_{max}. \quad (23)$$

Using these equations, it is clear that the short dipole moments create changes in both the input resistance, as well as radiated resistance. The modification that exists however, do not significantly change the directivity of the curved antenna, and therefore will not change the maximum effective area of the antenna itself. This proposition is a very interesting conceptual idea which proposes that the tag would have the same directivity measure as would, say a typical dipole under no curvature ($K = 0$). The theory also predicts that the effective capture area would not change drastically, thus the power radiated by the tag would also remain relatively constant. Since the radiation resistances change due to curvatures, it is probable to suggest that the operation of the tag would be dependent on these changes. For the typical passive UHF RFID tag, changes in the input resistance would create a mismatch with the tag ASIC load, which would detune the operational frequency of the tag. This act would effectively hover the typical tag away from its' operational frequency band of 902 MHz through to 928 MHz in the US. The effect of tag detuning is an analysis that is well known in passive tags, and has been previously discussed in relation to a metallic environment [4, 13], as well as in a moist environment [28]. In order to verify the results of the theory, simulations are conducted in FEKO 5.3, which is a CEM tool utilizing a hybrid FEM/MoM method. The meshing guidelines used here require that the segment radius equals to 10^{-4} m, and that the segment length equals to $\lambda/90$ m, which allows for the vastly assumed regions for the short dipole concepts of $< \lambda/50$ m.

Fig. 9 presents the test setup used in the simulation environment. Note that the values of curvature (K) is varied starting from $K = 0$ ($R = \infty$), up to $K = 4\pi/\lambda$, where the typical quarter wave dipole becomes a complete loop.

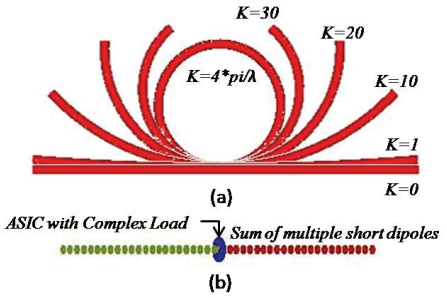

Fig. 9.Test setup of the curvature of a center-fed dipole: (a) showing the variation of curvature (K); (b) the tag composed of a summation of cylindrical parts and a complex load.

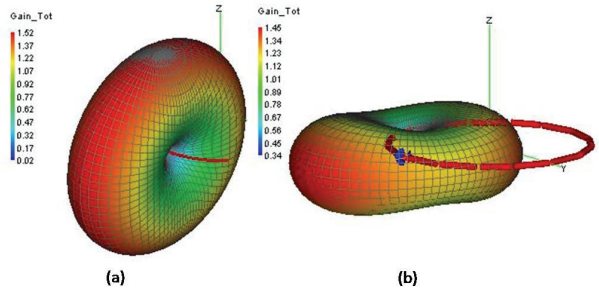

Fig. 10. 3D pattern of the tag gain: (a) during curvature values of $\boldsymbol{K < 4\pi/\lambda}$; (b) at $\boldsymbol{K = 4\pi/\lambda}$.

In Fig. 9b, we notice that the mathematical model utilized for the dipole involves a summation of cylindrical short dipoles, while the center feed point is an ASIC. In the simulation, the feed point is designed to be a sinusoidal voltage with a maximum value of 1V, and the point source is modeled using a complex load (real and imaginary parts). The values of the complex load are varied to achieve the optimal load for matching purposes. This process is repeated for each tag antenna design utilized in this paper (Alien Squiggle and Raflatac Bent Dipole). Fig. 10 depicts the 3D radiation patter of the curved dipole tag at normal curvature (close to the regular straight dipole

antenna), and at the extreme curvature (where the dipole becomes a loop antenna). Since the theory is designed to handle a dipole antenna (Equations 1 to 3), it is not sufficiently accurate at the maximum curvatures, and therefore is theoretically unsuited to accommodate loop like structures.

From Fig. 10, we notice that the tag maintains a dipole like pattern throughout various types of curvature, but transforms from an isotropic-x (or -y) into an isotropic-z as the tag approaches the maxima curvatures of $K = 4\pi/\lambda$. Fig. 11 presents the results indicating the effect of the curvature at different frequencies (using a frequency sweep). Here we notice that curvature (K) of a typical dipole has an impact on the frequency of operation of the tag. There is a skewing effect on the optimal operational frequency that seems to slide off to higher frequencies as the tag curvatures increase ($K \rightarrow 4\pi/\lambda$). However, at the maxima curvatures of $K = 4\pi/\lambda$, it is seen (yellow) that the tag offers very poor values of reflection coefficients (S_{11}), which could be related to due to the high voltage standing wave ratio (VSWR) when contact is made between each end of the tag.

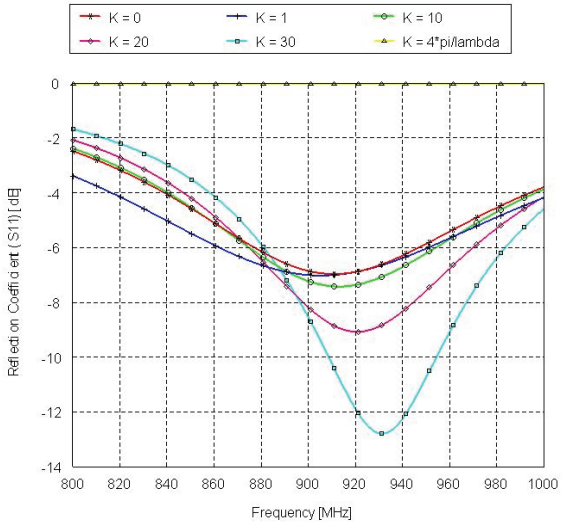

Fig. 11. Effect of curvature (***K***) at different frequencies.

Fig. 12 presents the effect of curvature on the optimal value of the imaginary load impedance. The imaginary load is varied for negative values of 1 through to 1000 Ω. From the logarithmic (x-axis) scale it is noticed that the imaginary part is well suited (for lowest S_{11} values) at values of approximately -50 Ω (for all values of curvatures, K). Note that throughout this paper, the real part of the complex load is affixed at 50 Ω. Using these values ($[50 - j50]$ Ω) for the analytical evaluation, Fig. 14 is derived to depict the effect of curvature on the fundamental RF parameters in the tag.

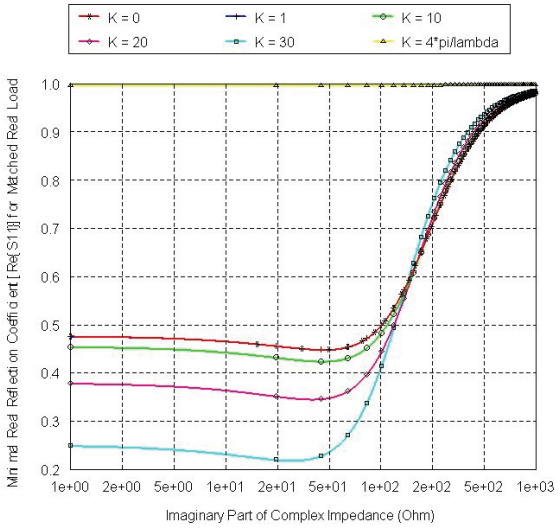

Fig. 12. Effect of curvature (***K***) on the optimal value for the imaginary part of the complex impedance of the load.

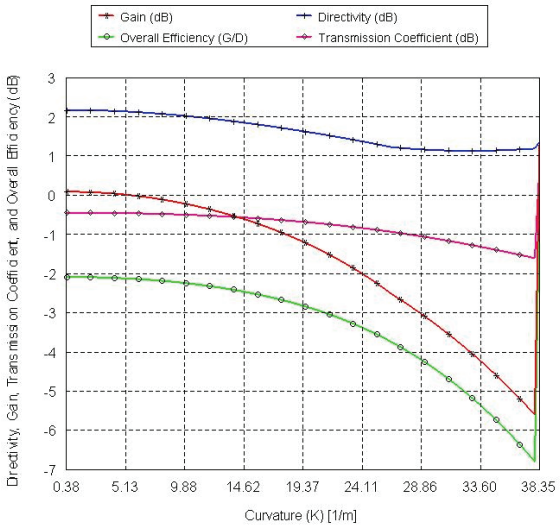

Fig. 13. Effect of curvature (***K***) on the directivity, gain, overall efficiency, and transmission coefficient of a center-fed dipole tag at 915 MHz.

The parameters derived from this analysis are the gain, directivity, overall efficiency, and transmission coefficient. Notice that the gain and

the directivity values are different (not the same) for tag curvatures above $K > 0$. This is an interesting idea when considering the definition of gain and directivity which often times reflects their similarities under the assumptions of a perfect match and no ohmic losses. However, the finer interest that lie in the differences here are the fact that the differences are in variation with respect to the curvature itself. This distorted case is what is of most interested, and can be easily described using the harmonized definition of gain and directivity as detailed in Equation 24.

$$G_T = (1 - |\Gamma|^2) \cdot D_T \,. \tag{24}$$

Using this refined definition, we notice that the transmission coefficient ($|\Gamma|$) is in fact frequency dependent, and as depicted in Fig. 14 plays a crucial role in the manipulation of the tag overall efficiency, a factor that changes the gain to be much lower than the directivity of the tag antenna itself. Fig. 15 compares the results of the transmission coefficient in Fig. 14 against values of the reflection coefficients, return loss, and VSWR. Here we see that as $|\Gamma|$ decreases with the curvature of a tag, the theory predicts that the return loss would also increase.

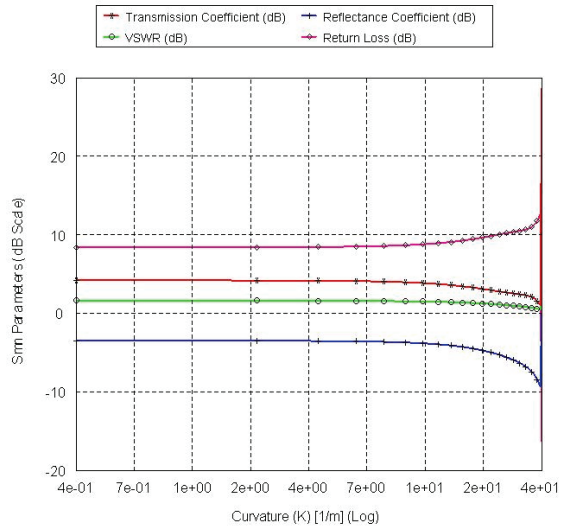

Fig. 14. Effect of curvature ($\boldsymbol{K}$) on the reflectance coefficient, voltage standing wave ratio, and return loss as compared to the transmission coefficient for a center-fed dipole tag at 915 MHz.

In understanding the implications of these results, we must draw attention to the fact that the range ratio of the passive tag can be effectively characterized using Equation 25.

$$\frac{R'}{R} = \sqrt{(1 - |\Gamma|^2)\frac{D'}{D}} \,. \tag{25}$$

Considering the fact that at values of $K < \pi/\lambda$ the change in directivity is negligible, we can generalize that the range ratio is dependent only on the values of the overall efficiency (e_{cd}) at these values as described by Equation 26.

$$\frac{R'}{R} = \sqrt{e_{cd}} \,. \tag{26}$$

It is seen that there exist an exponential account on the performance degradation of passive tags after this cutoff point, which contributes directly (through equation 26) to the readability of these tags.

V. EXPERIMENTAL ANALYSIS

The experimental analysis of curvature effects on the Alien Squiggle is conducted in free space (indoor). Fig. 15 depicts the test setup for the curvature analysis conducted in this section.

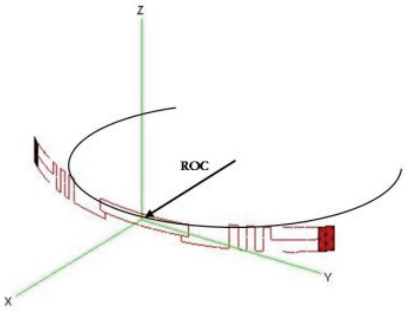

Fig. 15. Curvature setup of the Alien Squiggle tag for a given radius of curvature (ROC).

The analysis is first conducted to derive the optimal imaginary part of the tag, which is then compared with the bent dipole tag by Raflatac in Fig. 16. From this figure, we notice that the imaginary part of the Alien Squiggle is perfectly matched (the real part is 50 Ω) when the complex load is approximately ($[50 - j508.3]\Omega$). This value is also much lesser than that required for perfect matching (under the same conditions) of the Raflatac bent dipole at 915 MHz. Using the same simulation environment, Fig. 17 plots the effect of curvatures on the reflection coefficient (in dB) from 800 MHz through to 1000 MHz.

Here it is noticeable that there is a trend for the skew towards higher frequencies and higher reflection losses as the curvature of the tag increases. Fig. 18 presents the analysis conducted in free space using the actual tag.

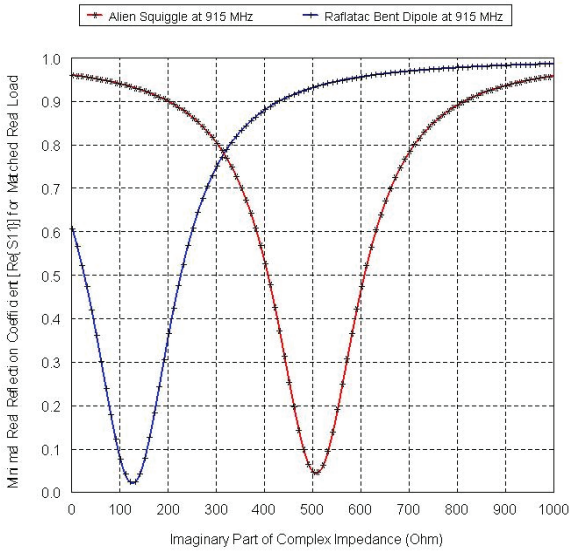

Fig. 16. Optimal value for the imaginary part of the complex load of the Alien Squiggle tag compared with the Raflatac bent dipole.

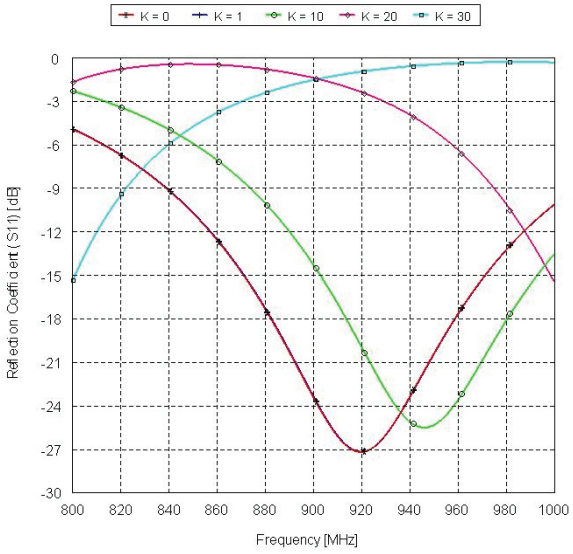

Fig. 17. Effects of curvature on variations of the reflection coefficient for the perfectly matched (at 915 MHz) Alien Squiggle tag from 800 MHz through to 1000 MHz.

It is seen that the fitted polynomial curves (darker lines) show that frequency skewing is less of a real issue, while losses are much more prevalent. The testing was conducted in open lab space without obstacles, and that a repeatability test was conducted to determine the extent of the noise and its' occurrences, which proved to be negligible. The global minima of the curves indicate the tuning of the tag which is compared to the reflection coefficient plots in Fig. 17, while the change in transmitted power required is related to the impedance mis-match due to the constant curvature of the tag. The test is conducted with heights of 1m from the ground for both the tag and reader antenna, and for a separation of 1m from each other. The ripples in the measured curves are a result of multi-path which is present in the testing environment.

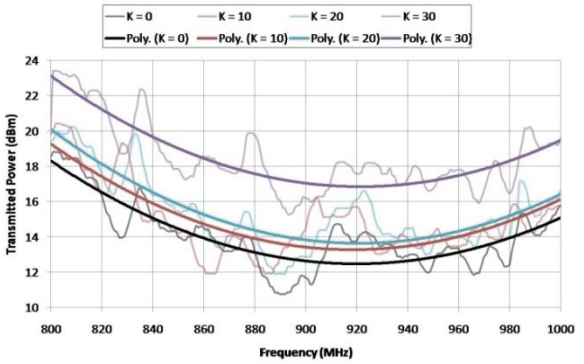

Fig. 18. Experimental analysis and polynomial curve fitting of the results for curvatures of the Alien Squiggle tag from 800-1000 MHz.

VI. EFFECTS OF THE SEGMENTATION PROCESS IN CEM TOOLS

It is shown that the current profile plays the most crucial role in the field equations, an occurrence that is studied in Fig. 7 in general, and detailed in Fig. 19 numerically.

As the number of segments (#) increases (lambda/#) in the theory, the normalized current becomes more sinusoidal in nature, which contributes to the accuracy of the theory. Increases in the curvature would definitely increase the effect that the segments play in the calculation of the field equations.

Fig. 20 shows that for a damp segmentation process (with higher segment counts), the breakdown begins at $K > 3\pi/\lambda$, and (from the previous sections) occurs at $K = 4\pi/\lambda$. In addition to these factors, we also predict that readability and performance is not effected (in

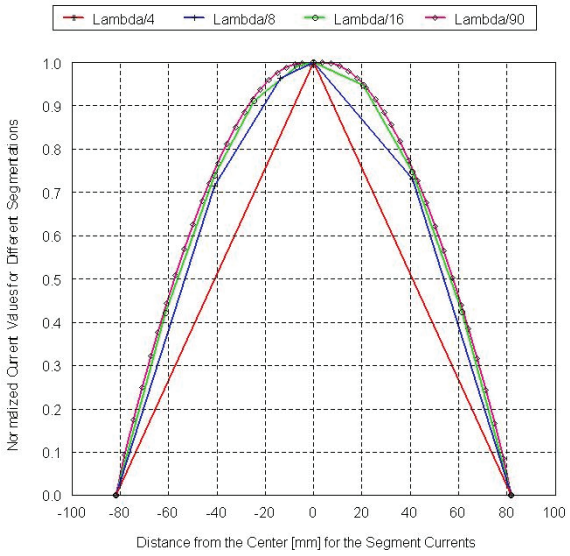

Fig. 19. Effect of the segmentation process and meshing guidelines on the segment currents.

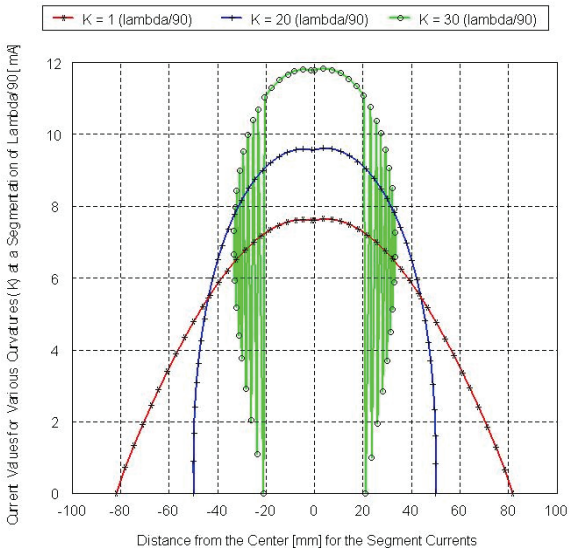

Fig. 20. Effect of the tag curvature on the segment currents for damp meshing guidelines (dense segmentation process).

ideal conditions) until $K > \pi/\lambda$ for a typical dipole-like passive UHF RFID tag antenna, where λ is the wave-length referred to the self-resonance of the antennas, rather than the frequency of operation of the tag. This is true since it is common to design passive UHF RFID tags away from the self resonance of the antenna, and due to the fact that K is related to the antenna directly.

VII. CONCLUSION

In this paper, a theoretical framework is presented to describe the effects of curvature on the passive RFID tag. Maxwell's equations are used to describe the curvature of the typical tag by using the center-fed dipole as a standard tag antenna. The equations are derived to present a general theory describing curvature in passive UHF RFID tags. Analytical evaluations are conducted to study the variation of gain, impedance mismatching, as well as operational frequency shifting of the passive UHF RFID tag. Experimental evaluations of curvature in commercially existing passive UHF RFID tags are conducted. The results of this study show that there exist significant impacts on the performance of the typical RFID tag at curvature values of $K > \pi/\lambda$. Furthermore, it is shown that a breakdown (non-conformity to typical operation) occurs at $K = 4\pi/\lambda$.

REFERENCES

[1] H. Vogt, "Efficient Object Identification with Passive RFID Tags", *Int. Conf. on Pervasive Computing*, No. 2424, pp. 98-113, 2002.

[2] R. Glidden, "Design of ultra-low-cost UHF RFID tags for supply chain applications", *IEEE Communication Magazine*, Vol. 42, No. 8, pp .140-151, 2004.

[3] P. V. Nikitin, K. V. S. Rao, and R. D. Martinez, "Differential RCS of RFID tag", *Electronics Letters*, Vol. 43, No. 8, pp. 431-432, 2007.

[4] D. D. Arumugam, D.W. Engels, and A. Modi, "Environmental and performance analysis of SAW-based RFID systems", *Int. J. Radio Frequency Identification Technology and Applications*, Vol. 1, No. 2, pp. 203-235, 2007.

[5] D. D. Arumugam, A. Vijayakrishnan, D. W. Engels, and A. Modi, "2D localisation using SAW-based RFID systems: a single antenna approach", *Int. J. Radio Frequency Identification Technology and Applications*, Vol. 1, No. 4, pp. 417-438, 2007.

[6] D. D. Arumugam, and D. W. Engels, "Characterization of RF Propagation in Helical and Toroidal Metal Pipes for Passive RFID Systems", *IEEE Int. Conf. on RFID*, Vol. 39, No. 1, pp. 61-62, 2008.

[7] D. D. Arumugam and D. W. Engels, "Characterisation of RF Propagation in Metal Pipes for Passive RFID Systems", *Int. J. Radio Frequency Identification Technology and Applications*, Vol. 1, No. 3, pp. 303-343, 2007.

[8] D. D. Arumugam and D. W. Engels, "Characterisation of RF Propagation in Rectangular Metal Pipes for Passive RFID Systems", *Int. J. Radio Frequency Identification Technology and Applications*, Vol. 1, No. 4, pp. 345-362, 2007.

[9] P. V. Nikitin and K. V. S. Rao, "Theory and measurement of backscattering from RFID tags", *IEEE Trans. on Antennas and Propagation*, Vol. 48, No. 6, pp. 212-218, 2006.

[10] K. V. S. Rao, "An overview of backscattered radio frequency identification system (RFID)", *Asia Pacific Microwave Conference*, Vol. 3, pp. 746-749, 1999.

[11] K. V. S. Rao, P.V. Nikitin, and S.F. Lam, "Antenna design for UHF RFID tags: A review and a practical application", *IEEE Trans. on Antennas and Propagation*, Vol. 53, No. 12, pp. 3870-3876, 2005.

[12] M. E. Schaffrath, L. Ukkonen, L. T. Sydanheimo, and M. A. Kivikoski, "RFID Antenna Designs for Paper Industry Applications: Passive Bow-Tie-Transponder Performance Analysis", *IASTED Int. Conf. on Antennas, Radar, and Wave Propagation*, pp. 348–353, 2005.

[13] L. Sydanheimo, L. T. Ukkonen, and M. Kivikoski, "Effects of Size and Shape of Metallic Objects on Performance of Passive Radio Frequency Identification", *IEEE/ACES Int. Conf. on Wireless Communications and Applied Computational Electromagnetics*, pp. 178-181, 2006.

[14] G. Kumar and K. P. Ray, *Broadband Microstrip Antennas*, Artech House, 2003.

[15] K. D. Laakmann and W. H. Steier, "Waveguides: Characteristic Modes of Hollow Rectangular Dielectric Waveguides," *Applied Optics*, Vol. 15, pp. 1334-1340, 1976.

[16] J. M. Molina-Garcia-Pardo, M. Lienard, P. Degauque, D. G. Dudley and L. Juan-Llacer, "MIMO Channel Characteristics in Rectangular Tunnels from Modal Theory," *IEEE Transactions on Vehicular Technology*, 2006.

[17] S. F. Mahmoud and J. R. Wait, "Guided Electromagnetic Waves in a Curved Rectangular Mine Tunnel," *Radio Science*, Vol. 9, pp. 567-572, 1974.

[18] M. A. K. Hamid, W. M. Boerner, L. Shafai, S. J. Towaij, W. P. Alsip, and G. J. Wilson, "Radiation Characteristics of Bent-Wire Antennas", *Electromagnetic Compatibility, IEEE Transactions on,* Vol. 12, No. 3, pp. 106-111, Aug. 1970.

[19] G. Burrell, " Propagation of current on bent wire antennas-an experimental study", *Antennas and Propagation, IEEE Transactions on,* Vol. 26, No. 3, pp. 427-434, May 1978.

[20] S. Egashira, M. Taguchi, and A. Sakitani, "Consideration on the measurement of current distribution on bent wire antennas", *Antennas and Propagation, IEEE Transactions on,* Vol. 36, No. 7, pp. 918-926, July 1988.

[21] S. Y. Y. Leung and D. C. C. Lam, "Performance of Printed Polymer-Based RFID Antenna on Curvilinear Surface", *Electronics Packaging Manufacturing, IEEE Transactions on,* Vol. 30, No. 3, pp. 200-205, July 2007

[22] X. Zhou and G. Wang, "Study on the influence of curving of tag antennas on performance of RFID system," *4th International Conference on Microwave and Millimeter Wave Technology Proceedings* (IEEE Cat. No.04EX827), pp. 122-125, 2004.

[23] H.-T. Hsu, H.-T. Chou, and W.-W. Lee, "Performance degradation of RFID system due to curving in tag antenna through Radar Cross Section (RCS) analysis," *2007 IEEE Antennas and Propagation Society International Symposium,* pp. 1197-2000, 2008.

[24] Y. Tikhov and J. H. Won, "Impedance-matching arrangement for microwave transponder operating over plurality of bent installations of antenna," *Electronics Letters,* Vol. 40, No. 10, pp. 574-575, May 2004.

[25] J. Siden, P. Jonsson, T. Olsson, and G. Wang, "Performance degradation of RFID system due to the distortion in RFID tag antenna", Microwave and Telecommunication Technology, 11th International Conference on, pp. 371-373, 2001.

[26] C. A. Balanis, *Antenna Theory: Analysis and Design*, John-Wiley and Sons Publishing Company, 2005.
[27] D. K. Cheng, *Fundamentals of Engineering Electromagnetics*, Addison-Wesley Publishing Company, 1993.
[28] R. Fletcher, U. P. Marti, and R. Redemske, "Study of UHF RFID signal propagation through complex media", *IEEE Int. Symp. on Antennas and Propagation Society*, Vol. 1B, pp. 747-750, 2005.

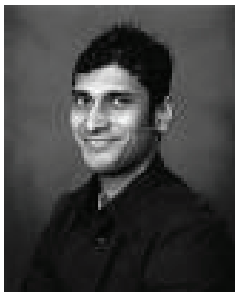

Darmindra D. Arumugam is a Researcher and a Ph.D. Candidate in the Department of Electrical & Computer Engineering at Carnegie Mellon University. He received a BSc and MSc in Electrical Engineering at the University of Texas at Arlington in 2005 and 2007. His current research is in the area of applied physics and electromagnetism concentrating on radiation theory and propagation characteristics, applications of smart objects and sensors, energy harvesting, wireless sensor networks and intelligent objects. Mr. Arumugam has authored over 30 peer reviewed international journal and conference publications, and has been invited to speak at numerous technical events.

Daniel W. Engels is the Director of the Texas Radio Frequency Innovation and Technology Center and an Associate Professor at the University of Texas at Arlington. Dr. Engels is the former Director of Research of the Auto-ID Labs at MIT and is an original member of the research team started in 1998 that founded the Auto-ID Center at MIT. Dr. Engels is one of the principal architects of the Networked Physical World EPC System, the foundation of the Internet of Things, developed under the Auto-ID Center and licensed to EPCglobal Inc. Dr. Engels received his Ph.D. from the Massachusetts Institute of Technology. He has over 50 peer reviewed publications in RFID, RFID applications, security, embedded computing, and computer-aided design.

Marlin H. Mickle is Nickolas A. DeCecco Professor in Electrical and Computer Engineering (Primary), Professor of Computer Engineering, Telecommunications, and Industrial Engineering at the University of Pittsburgh. He is the Director of the RFID Center of Excellence. He received the B.S.E.E., M.S.E.E., and the Ph.D. University of Pittsburgh in 1961, 1963, and 1967. Marlin received the Carnegie Science Center Award for Excellence in Corporate Innovation - 2005; he has 21 patents and received the Pitt Innovator Award 2005, 2006, 2007 and 2008; 1988 Recipient of the Systems Research and Cybernetics Award of the IIASSRC, a member of the AIDC100, and he is a Life Fellow of the IEEE.